Rheol Acta (2017) 56:369–376
DOI 10.1007/s00397-017-1000-9

ORIGINAL CONTRIBUTION

A modified lattice boltzmann method for herschel-bulkley fluids

Weiwei Wu[1] · Xiaodiao Huang[1] · Hong Yuan[1] · Fei Xu[1] · Jingtao Ma[2]

Received: 27 October 2016 / Revised: 7 February 2017 / Accepted: 8 February 2017 / Published online: 20 February 2017

Abstract As one kind of the most important non-Newtonian fluids, Herschel-Bulkley fluids have been applied in practical engineering widely. In order to improve the stability and accuracy in the simulation of Herschel-Bulkley fluids with lattice Boltzmann method (LBM), a modified lattice Boltzmann method was proposed. With Poiseuille flow as the example, the shear-thinning fluids and the shear-thickening fluids were used, respectively, to introduce the method in detail. The comparison between the velocity distributions and the analytical solutions demonstrated the feasibility of the modified method. Also the effect of the power law index, lattice nodes, and the region of the shear rate on the relative error was discussed. Then, the method was applied into the simulation of the cement paste flow in the 3D printing extruder. The streamline figure was obtained and then conducted the flow simulation by the modified method and multiple-relaxation-time lattice Boltzmann method (MRT-LBM), respectively; the comparison further proved the modified method was feasible for Herschel-Bulkley fluids.

Keywords Herschel-Bulkley fluids · A modified lattice Boltzmann method · Poiseuille flow · Cement 3D printing

✉ Xiaodiao Huang
njtechhxd@126.com

[1] School of Mechanical and Power Engineering, Nanjing Tech University, Nanjing, Jiangsu, 211800, People's Republic of China

[2] School of Engineering and Information Technology, University of New South Wales, Canberra, ACT 2600, Australia

Introduction

Lattice Boltzmann method (LBM) is evolved from lattice gas automata, which has been widely applied in engineering thermophysics, mechanics, electrical, medical, and other related fields. Researchers have studied the theory, model, and application deeply, which promote the development and application of LBM widely (Sheikholeslami et al. 2014; Ashorynejad et al. 2013; Shen et al. 2003; Wang et al. 2011; Guo et al. 2005; Yuan and Rahman 2016; Zhang et al. 2008; Boyd et al. 2007).

The evolution process of LBM is achieved by two steps: streaming and collision. The computational process is simple and stable, meanwhile the physical process is clear and easy to realize, which both make LBM widely applied in the fluids fields. To ensure the stability and accuracy, many people propose improvements, such as multiple-relaxation-time lattice Boltzmann method (MRT-LBM; D'Humières 2002; Zhen-Hua et al. 2006), entropy lattice Boltzmann method (Ansumali and Karlin 2002a, b; Spasov et al. 2009), and other methods combine with the finite methods (Kefayati 2014a, b; Seta and Takahashi 2002); they promote rapid development of LBM. Also LBM provides a new thought for the simulation of the non-Newtonian fluids. J.M. Buick analyzed the flow of the power law fluids in the single screw with LBM. The solution shows that the flow is considerably influenced by the non-Newtonian behavior (2009); Chai Zhenhua simulated the flow of power law fluids and Bingham fluids by MRT-LBM, which showed an excellent stability and accuracy (2011). On simulating non-Newtonian fluids flow, the relaxation time influences the stability and accuracy directly, which limits the application of LBM in the non-Newtonian fluids flow. So Gabbanelli presented a truncated model for power law fluids and tested its effectiveness by Poiseuille flow (2005); Malaspinas conducted a

local method on power law fluids and Carreau fluids, which showed a good stability within a certain range of power index (2007); and Boyd took the local method to simulate the power law flow in the tunnel. The research proves that there is a better accuracy and efficiency than the truncated method proposed by (Boyd et al. 2006).

Many studies have been done on the stability and accuracy of the non-Newtonian fluids by LBM, but the focus is always on the common fluid types such as power law fluids and Bingham fluids, which lacks to the deep investigation of the unusual non-Newtonian fluid types like Herschel-Bulkley fluids.

In this paper, a modified model was proposed for Herschel-Bulkley fluids, which was based on the similarity between Bingham fluids and Herschel-Bulkley fluids. Then Poiseuille flow was taken to make a comparison and error analysis within different power law indexes. Finally, it was applied to simulate the cement paste flow in 3D printing extruder. The solution obtained by the method was compared with the result of MRT-LBM.

Modified lattice Boltzmann method

Lattice Boltzmann method for Herschel-Bulkley fluids

An entire LBM model consists of three parts: discrete velocity model, equilibrium distribution function, and evolution equation of the distribution function.

The evolution equation of the distribution function is defined as:

$$f_i(\mathbf{r}+\mathbf{e}_i\delta t, t+\delta t)-f_i(r,t)=-\frac{1}{\tau}\left[f_i(\mathbf{r},t)-f_i^{eq}(r,t)\right] \tag{1}$$

where τ is the relaxation time, as the time interval between two collision steps (Chai et al. 2011).

The evolution equation can be divided into equilibrium and non-equilibrium. So Eq. 1 can also be described as:

$$f_i = f_i^{eq} + \varepsilon f_i^{neq} \tag{2}$$

With the technique of the Chapman-Enskog expression, Eq. 2 can be expanded up to second order with respect to the parameter ε as:

$$f_i = f_i^{eq} + \varepsilon f_i^{(1)} + \varepsilon^2 f_i^{(2)} + o(\varepsilon^3) \tag{3}$$

For the non-Newtonian fluids, the rate-of-strain tensor can be derived according to the momentum tensor as:

$$S_{\alpha\beta} = -\frac{1}{2\rho\tau c_s^2}\sum_{i=0}^{8} e_{i\alpha}e_{i\beta}\varepsilon f_i^{(1)} \tag{4}$$

The second invariant of the rate-of-strain tensor can be obtained through Eq. 4 as:

$$D_{II} = \sum_{\alpha,\beta=1}^{l} S_{\alpha\beta}S_{\alpha\beta} \tag{5}$$

where l is the dimension, here $l = 2$. The shear rate can be derived through Eq. 5 as (Buick 2009):

$$\dot{\gamma} = \sqrt{2D_{II}} \tag{6}$$

The constitutive model of Herschel-Bulkley fluids is defined as:

$$\tau_a = \begin{cases} \tau_0 + K\dot{\gamma}^n & , |\tau| > \tau_0 \\ \dot{\gamma} = 0 & , |\tau| < \tau_0 \end{cases} \tag{7}$$

To avoid the inconvenience of the piecewise function in the simulation, the modified constitutive model is taken as:

$$\tau_a = \tau_0[1-\exp(-m\dot{\gamma})] + K\dot{\gamma}^n \tag{8}$$

where m controls the increase of the stress, which can avoid the discontinuous of the constitutive equation. When it tends to be zero, the equation is the constitutive equation of the power law fluids. While it tends to be infinity, the equation will be the constitutive equation of ideal Herschel-Bulkley fluids. In this paper, $m = 500$. It is worth noting that m cannot be selected as larger enough randomly, or the divergence will produce. The apparent viscosity coefficient can also be obtained by further derivation as (Mitsoulis 2007; Papanastasiou and Boudouvis 1997; Alexandrou et al. 2001):

$$\nu_{ap} = K|\dot{\gamma}|^{n-1} + \frac{\tau_0}{|\dot{\gamma}|}[1-\exp(-m|\dot{\gamma}|)] \tag{9}$$

The relationship between kinematic viscosity ν and the relaxation time is given by:

$$\nu = \frac{2\tau\text{-}1}{6}c^2\delta t \tag{10}$$

With Eq. 10, we can obtain the local apparent relaxation time τ_{ap}, then replacing the relaxation time τ in Eq. 1 for the following simulation.

The modified LBM for Herschel-Bulkley fluids

According to the above statement, when LBM is applied into the simulation of the non-Newtonian fluids, the process mainly depends on the local relaxation time, which can also be viewed as it is affected by the viscosity, while the viscosity associates with the rate-of-strain via stress tensor. For Herschel-Bulkley fluids, when $n < 1$, the case corresponds to shear-thinning fluids; $n = 1$, recovers Bingham behavior; and $n > 1$, corresponds to shear-thickening fluids. When LBM is applied into the non-Newtonian fluids directly, the process may be unstable and the accuracy will be low. With the shear rate close to zero, for the shear-thinning fluids, the

viscosity will be infinity, which will result in divergence, while for the shear-thickening fluids, the viscosity will turn to zero. In the previous research, there is no solution that has been proposed for Herschel-Bulkley fluids to solve the above problems.

In fact, most of the non-Newtonian fluids show the non-Newtonian behavior just in a certain range of rate-of-shear; otherwise, they behave like Newtonian fluids, which means that the viscosity is a constant when the rate-of-shear is out of the range (Gabbanelli et al. 2005). Based on this, a modified method is proposed for Herschel-Bulkley fluids, which is expressed as a piecewise function. Because of the yield stress, and to make sure the viscosity is a constant, when the rate-of-shear is out of the range, we replace the constitutive model with that of Bingham fluids

$$\nu(\dot{\gamma}) = \begin{cases} \tau_0/\dot{\gamma}_0 + \mu_B \dot{\gamma}_0^{(n-1)} & , \dot{\gamma} < \dot{\gamma}_0 \\ \tau_0/\dot{\gamma} + K\dot{\gamma}^{(n-1)} & , \dot{\gamma}_0 < \dot{\gamma} < \dot{\gamma}_\infty \\ \tau_0/\dot{\gamma}_\infty + \mu_B \dot{\gamma}_\infty^{(n-1)} & , \dot{\gamma} > \dot{\gamma}_\infty \end{cases} \tag{11}$$

The simulation will be stable and accurate when the kinematic viscosity is in a certain range. If the relaxation time is close to 1/2, the process of LBM will be unstable, and the corresponding viscosity is close to zero, $\nu \leq 0.001$; Conversely, the accuracy will be low while the relaxation time is larger than 1 and the corresponding viscosity is relatively large, $\nu \geq 1/6$. As a result, we set the limit values of the viscosity: $\nu_{\min} = 0.001$ and $\nu_{\max} = 1/6$. Clearly, the upper limit value of the viscosity corresponds to the case that the rate-of-shear is close to zero for the shear-thinning fluids; meanwhile, the lower limit value of viscosity corresponds to the case that the rate-of-shear is close to zero for the shear-thickening fluids (Gabbanelli et al. 2005; Conrad et al. 2014).

Flow between parallel plates

The Poiseuille flow is always chosen to test the stability and accuracy of LBM (Wang and Ho 2008; Pontrelli et al. 2009). Here, we take Poiseuille flow as an example to introduce the modified method in detail. The distance of two parallel plates along y direction is H and there is a pressure gradient ∇P along x direction. We can obtain the distribution of the velocity u_y along $y$direction. We divide the distance into $[-H/2, 0]$ and $[0, H/2]$. According to the symmetry, we just need to simulate the case in $[0, H/2]$ so that the solution of another part can also be obtained. In the interval $[0, H/2]$, we can divide it into four regions: A, B, C, and D. The region A corresponds to the high-shear-rate area close to the wall, where the shear rate exceeds $\dot{\gamma}_\infty$, and y_h is the cutoff value. The fluids can be viewed as Bingham fluids in this region. And the region B corresponds to the effective area of Herschel-Bulkley fluids, and y_l is the cutoff value. The region C corresponds to the low-shear-rate area; the fluids in this region can also be viewed as Bingham fluids. In region D, the stress is lower than the yield stress; here, the shear rate is zero and y_τ is the cutoff value. Combined with the velocity derivation of Poiseuille flow, the analytical solution can be obtained as:

$$u_y = \begin{cases} \frac{n}{n+1}\left(-\frac{1}{K}\frac{\partial P}{\partial x}\right)^{1/n}\left[\left(\frac{H}{2}+\frac{\tau_0}{\partial P/\partial x}\right)^{(n+1)/n} - \left(y_\tau + \frac{\tau_0}{\partial P/\partial x}\right)^{(n+1)/n}\right] & , 0 \leq y \leq y_\tau \\ -\frac{1}{2\nu_0\rho}\frac{\partial P}{\partial x}\left[\left(\frac{H}{2}+\frac{\tau_0}{\partial P/\partial x}\right)^2 - \left(y + \frac{\tau_0}{\partial P/\partial x}\right)^2\right] + \alpha_1 & , y_\tau \leq y \leq y_l \\ \frac{n}{n+1}\left(-\frac{1}{K}\frac{\partial P}{\partial x}\right)^{1/n}\left[\left(\frac{H}{2}+\frac{\tau_0}{\partial P/\partial x}\right)^{(n+1)/n} - \left(y + \frac{\tau_0}{\partial P/\partial x}\right)^{(n+1)/n}\right] + a_2 & , y_l \leq y \leq y_h \\ -\frac{1}{2\nu_\infty\rho}\frac{\partial P}{\partial x}\left[\left(\frac{H}{2}+\frac{\tau_0}{\partial P/\partial x}\right)^2 - \left(y + \frac{\tau_0}{\partial P/\partial x}\right)^2\right] + \alpha_3 & , y_h \leq y \leq H/2 \end{cases} \tag{12}$$

where the expressions of constant terms α_1, α_2, and α_3 can be derived as:

$$\begin{aligned} \alpha_1 &= \frac{n}{n+1}\left(-\frac{1}{K}\frac{\partial P}{\partial x}\right)^{1/n}\left[\left(\frac{H}{2}+\frac{\tau_0}{\partial P/\partial x}\right)^{(n+1)/n} - \left(y_\tau+\frac{\tau_0}{\partial P/\partial x}\right)^{(n+1)/n}\right] \\ &\quad + \frac{1}{2\nu_0\rho}\frac{\partial P}{\partial x}\left[\left(\frac{H}{2}+\frac{\tau_0}{\partial P/\partial x}\right)^2 - \left(y_\tau+\frac{\tau_0}{\partial P/\partial x}\right)^2\right] \\ \alpha_2 &= -\frac{1}{2\nu_0\rho}\frac{\partial P}{\partial x}\left[\left(\frac{H}{2}+\frac{\tau_0}{\partial P/\partial x}\right)^2 - \left(y_l+\frac{\tau_0}{\partial P/\partial x}\right)^2\right] \\ &\quad - \frac{n}{n+1}\left(-\frac{1}{K}\frac{\partial P}{\partial x}\right)^{1/n}\left[\left(\frac{H}{2}+\frac{\tau_0}{\partial P/\partial x}\right)^{(n+1)/n} - \left(y_l+\frac{\tau_0}{\partial P/\partial x}\right)^{(n+1)/n}\right] + \alpha_1 \\ \alpha_3 &= \frac{n}{n+1}\left(-\frac{1}{K}\frac{\partial P}{\partial x}\right)^{1/n}\left[\left(\frac{H}{2}+\frac{\tau_0}{\partial P/\partial x}\right)^{(n+1)/n} - \left(y_h+\frac{\tau_0}{\partial P/\partial x}\right)^{(n+1)/n}\right] \\ &\quad + \frac{1}{2\nu_\infty\rho}\frac{\partial P}{\partial x}\left[\left(\frac{H}{2}+\frac{\tau_0}{\partial P/\partial x}\right)^2 - \left(y_h+\frac{\tau_0}{\partial P/\partial x}\right)^2\right] + \alpha_2 \end{aligned} \tag{13}$$

With the taking of the derivative of the function of velocity distribution, the cutoff values can be obtained according to the equality of the stress.

$$\begin{aligned} y_\tau &= -\frac{\tau_0}{\partial P/\partial x} \\ y_l &= -\frac{1}{\partial P/\partial x}\left[\left(\frac{(\rho\nu_0)^n}{K}\right)^{1/(n-1)} - \tau_0\right] \\ y_h &= -\frac{1}{\partial P/\partial x}\left[\left(\frac{(\rho\nu_\infty)^n}{K}\right)^{1/(n-1)} - \tau_0\right] \end{aligned} \tag{14}$$

where $\partial P/\partial x = \nabla P$, we can get the region division according to the above expressions. It is important to note that the yield stress should satisfy $\tau_0 < \frac{1}{2}\left(\frac{(\rho\nu_0)^n}{K}\right)^{1/(n-1)}$ to ensure y_h is in the valid range.

In order to consider the effectiveness of the different power law indexes n in the truncated function, we take the range of n as $0.2 \sim 5$. The case $n < 1$ corresponds to shear-thinning fluids; here, we choose$n = 0.4$ and $n = 0.8$. While the case $n > 1$ corresponds to shear-thickening fluids, we choose $n = 1.5$ and $n = 2.0$. When $n = 0.4$, the pressure gradient is $\nabla P = -8.71 \times 10^{-5}$, the viscosity coefficient is $K = 0.000253$, the height of two parallel plates is $H = 1$, the lattice number is 96, and the density of the fluids is $\rho = 1$. The limit value of the kinematic viscosity is $\nu_{\min} = 0.001$ and $\nu_{\max} = 0.16$. When $n < 1$, there is $\nu_0 = 0.16$ and $\nu_\infty = 0.001$. The yield stress is $\tau_0 = 7.26 \times 10^{-6}$. Applying (12) into the analysis, we can get the velocity distribution as shown in Fig. 1. It is noted that y_h is not in the valid range, which resulted in the inexistence of the high-shear-rate region A. The solid lines correspond to the velocity distribution which obtained from Eq. 13. The circles are the solutions of the simulation. The dashed lines are the continuations of Herschel-Bulkley fluids and Bingham fluids. The vertical dashed lines correspond to the transition points.

When the power law index is $n = 1.5$, the pressure gradient is $\nabla P = -2 \times 10^{-4}$, the viscosity coefficient is $K = 0.0042$, the lattice number is 96, and the density of the fluids is $\rho = 1$. When $n > 1$, there is $\nu_0 = 0.001$ and $\nu_\infty = 0.16$. The yield stress is $\tau_0 = 2 \times 10^{-5}$. Applying (12) into the analysis, we can get the velocity distribution as shown in Fig. 2. It is noted that $y_h$is not in the valid range, which resulted in the inexistence of the high-shear-rate region A. The solid line corresponds to the velocity distribution which obtained from Eq. 13, the circles are the solution of the simulation, the dashed lines are the continuations of Herschel-Bulkley fluids and Bingham fluids, and the vertical dashed lines correspond to the transition points.

Comparing the gap between the dashed line and solid line in Fig. 1 with that in Fig. 2, the results show that the error between the analytical solution and numerical solution is

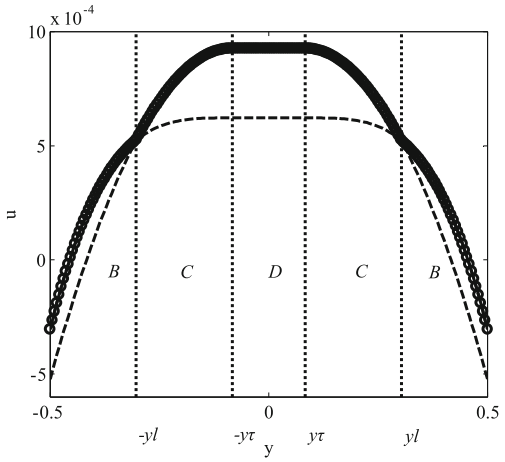

Fig. 1 Velocity distribution for $n = 0.4$

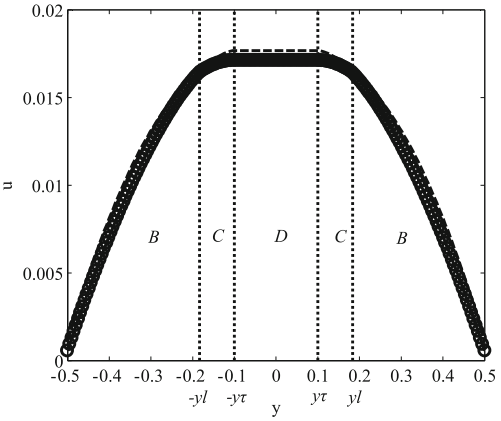

Fig. 2 Velocity distribution for $n = 1.5$

small while the region C is small. The region D depends on the yield stress τ_0 and the pressure gradient ∇P.

We run a series of simulations for the fluids at four different power law indexes. The lattice number is increased from 10 to 96 to compare the overall relative error between the solutions of the simulation and that of analytical. The relative error of the whole region is expressed as $\sum_{i=1}^{N}(1 - \nu_i^{LBM}/\nu_i^{anal})^2$. The accuracy depends on the viscosity, and the viscosity is expressed as $\nu^* = \nu(\delta x^2/\delta t)$. In order to ensure that the relative error discussed here is just related with the lattice number, we make $\delta x^2 = \delta t$. In this way, when the lattice number is increased, the viscosity can remain the same. Because the lattice space is $\delta x = 1/N$, the time step is $\delta t = 1/N^2$ according to the previous expression. Here, the lattice space changes from 1/10 to 1/96. The relative errors are calculated as shown in Fig. 3 with the increasing of the lattice number for different power law indexes. The solid line presents a line slope -1. Also the influence of different region magnitudes on the overall relative error is considered. Two different conditions are

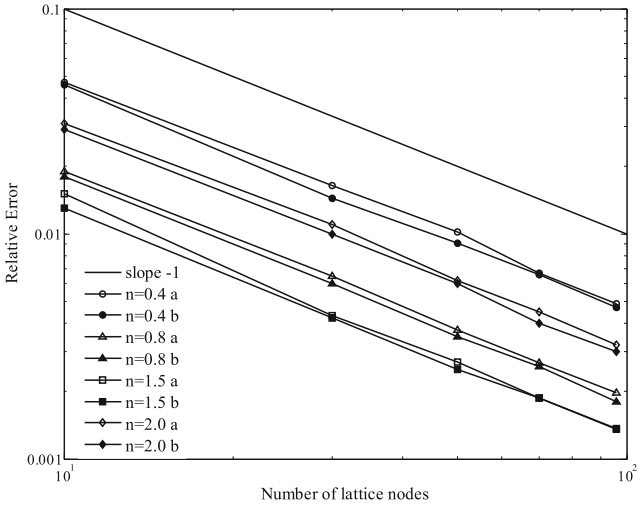

Fig. 3 Error analysis

discussed: a and b in each power index n. For condition a, which corresponds to the low-shear-rate region C is small, and for condition b, which covers the low-shear-rate region C is large, which is achieved by changing the pressure gradient ∇P. According to Eq. 14, when the magnitude of region C changes with the pressure gradient ∇P, the magnitudes of the other regions also change. It is important to note that when calculating y_h according to Eq. 14, it is always not in the valid range, which will result in the inexistence of the high-shear-rate region A. Only B, C, and D regions can be found in the figures. By comparison, the variation tendency of relative errors is almost the same in the case of a and b, and with the increasing of the lattice number, the relative error decreases. When the lattice number is continuously increased, the error will be controlled to less than 0.1 %. It can also be obtained that the difference of the error is apparent for different power law indexes n.

Application in the screw extruder of cement 3D printing

3D printing has been successfully applied into the architecture fields (Pegna 1997; Cesaretti et al. 2014; Zocca et al. 2015). And we also make a plan to research the cement 3D printing. The screw extruding is intended to be used for the modeling of the cement paste in 3D printing. The extruding device of the cement 3D printing consists of two parts: the screw extruder and the nozzle. It is important to understand the flow of the cement paste in the screw extruder. When the ratio is in a certain range, the cement paste can be viewed as Herschel-Bulkley fluids. As the temperature is 20 °C, and the hydration time is 5 min, the fluids will exhibit typical Herschel-Bulkley characteristics. The rheological equation can be described as Cruz and Pinho (2012):

$$\tau_a = \begin{cases} 3.899 + 1.103\dot{\gamma}^{0.633} & , |\tau_a| > 3.899 \\ \dot{\gamma} = 0 & , |\tau_a| < 3.899 \end{cases} \tag{15}$$

Transform (15) into the expression like (8). The parameter m is mainly used to control the increasing of the stress, when m is 500, the formula can be described as:

$$\tau = 3.899[1 - \exp(-500\dot{\gamma})] + 1.103\dot{\gamma}^n \tag{16}$$

The cement paste that flows through the area is shown in Fig. 1 when the screw rotates at a constant speed N. Assuming the screw is still, the barrel can be considered to contrarotate at the same speed N. Ignoring the incline of the screw flight (Kim and Kwon 1995), a cavity can be made when the flow fully expands the extruder (Sastrohartono et al. 1995), which can be seen in Fig. 5. Therefore, the analysis of the flow in the screw extruder as seen in Fig. 4 can be converted to the simulation of the cavity as seen in Fig. 5.

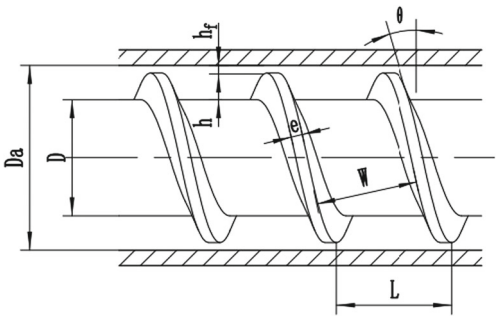

Fig. 4 Extruder structure

The initial speed is set only at the upper wall. The direction of the speed along Z is at $y = h$, and the speeds of the other three walls are set as 0 and the wall slip is ignored here. The actual geometry size of the section is $W = 16$ mm and $h = 6$ mm, and the lattice numbers are 288×108. Combining the scanning speed of the extruder with the curing time of the cement paste, the extrusion velocity is smaller than when it is applied in the polymer manufacturing field. Here, the rotation speed is adopted as $r = 30\text{min}^{-1}$ and the lead angle of the screw is $\theta = 20°$. With the similarity criterion, Reynolds number Re is taken as the key criterion number to transform the dimension, and other parameters also can be obtained. Then modify the viscosity according to Eq. 10 to guarantee the stability and accuracy.

In order to make a comparison, we choose MRT-LBM to simulate the flow. The function of MRT-LBM is expressed as:

$$\boldsymbol{f}(\boldsymbol{r} + \boldsymbol{e_i}\delta t, t + \delta t) - \boldsymbol{f}(\boldsymbol{r}, t) = -\boldsymbol{M}^{-1}\bar{\boldsymbol{S}}\boldsymbol{M}\left[\boldsymbol{f}(\boldsymbol{r}, t) - \boldsymbol{f}^{\boldsymbol{eq}}(\boldsymbol{r}, t)\right] \tag{17}$$

where $\boldsymbol{f}(\boldsymbol{r},t)$ denotes the density distribution function as the particle moves at the position $\boldsymbol{r}$ with the speed of $\boldsymbol{e_i}$ in time t and $\boldsymbol{f}^{eq}(\boldsymbol{r},t)$ is the equilibrium distribution function of $\boldsymbol{f}(\boldsymbol{r},t)$. $\boldsymbol{M}$ is the transfer matrix, which can transfer $\boldsymbol{f}(\boldsymbol{r},t)$ and

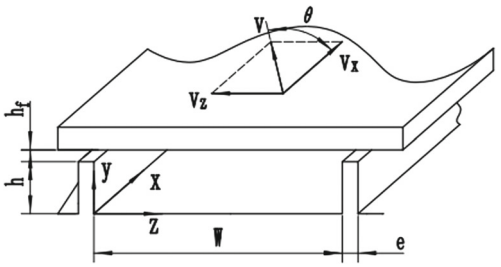

Fig. 5 Expansion structure

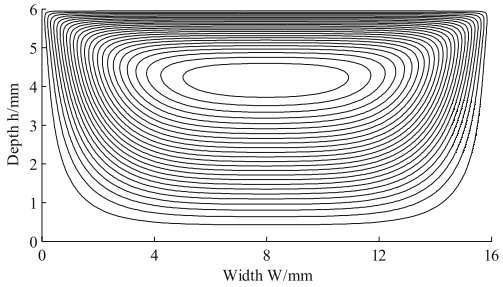

Fig. 6 Streamlines

$\boldsymbol{f}^{eq}(\boldsymbol{r},t)$ into moment space $\varrho(\boldsymbol{r},t)$ and $\varrho^{eq}(\boldsymbol{r},t)$, so $\varrho(\boldsymbol{r},t) = \boldsymbol{M}\boldsymbol{f}(\boldsymbol{r},t)$ and $\varrho^{eq}(\boldsymbol{r},t) = \boldsymbol{M}\boldsymbol{f}^{eq}(\boldsymbol{r},t)$. The matrix $\boldsymbol{M}$ is defined as:

$$\boldsymbol{M} = \begin{bmatrix} 1 & 1 & 1 & 1 & 1 & 1 & 1 & 1 & 1 \\ -4 & -1 & -1 & -1 & -1 & 2 & 2 & 2 & 2 \\ 4 & -2 & -2 & -2 & -2 & 1 & 1 & 1 & 1 \\ 0 & 1 & 0 & -1 & 0 & 1 & -1 & -1 & 1 \\ 0 & -2 & 0 & 2 & 0 & 1 & -1 & -1 & 1 \\ 0 & 0 & 1 & 0 & 1 & 1 & 1 & -1 & -1 \\ 0 & 0 & -2 & 0 & -2 & 1 & 1 & -1 & -1 \\ 0 & 1 & -1 & 1 & -1 & 0 & 0 & 0 & 0 \\ 0 & 0 & 0 & 0 & 0 & 1 & -1 & 1 & -1 \end{bmatrix}$$

$\overline{\boldsymbol{S}}$ is a diagonal matrix about the relaxation, which is defined as:

$$\overline{\boldsymbol{S}} = diag(s_0, s_1, s_2, s_3, s_4, s_5, s_6, s_7, s_8) \tag{18}$$

The density and the momentum are conserved quantities, so the relevant quantities s_0, s_3, and s_5 are 0, s_7, s_8 which are all equal to $1/\tau$, where τ is relaxation time of BGK model. The rest parameters are taken as a little bit bigger than 1, here $s_1 = s_2 = 1.4$, $s_4 = s_6 = 1.2$. The evolution of MRT includes streaming step and collision step. The collision step is different from that of BGK model as:

$$\boldsymbol{f}^{+}(\boldsymbol{r},t) = \boldsymbol{f}(\boldsymbol{r},t) - \boldsymbol{M}^{-1}\overline{\boldsymbol{S}} \tag{19}$$

where $\boldsymbol{f}^{+}(r,t)$ is the density distribution function after collision step. And the streaming step is the same as that of BGK model (Buick and Cosgrove 2006; Mohamad 2011).

The streamlines and velocity distributions can be obtained from the simulation. The streamlines is shown in Fig. 6. Affected by the viscosity and the structure, the paste flow in the extruder appears to be a circumfluence and the center of the circumfluence is at ($W = 0.5$, $h = 0.7$). There is no flow at the corner of the left bottom and right bottom. The velocity distributions are compared with that obtained by modified method, which are shown

Fig. 7 Velocity distributions

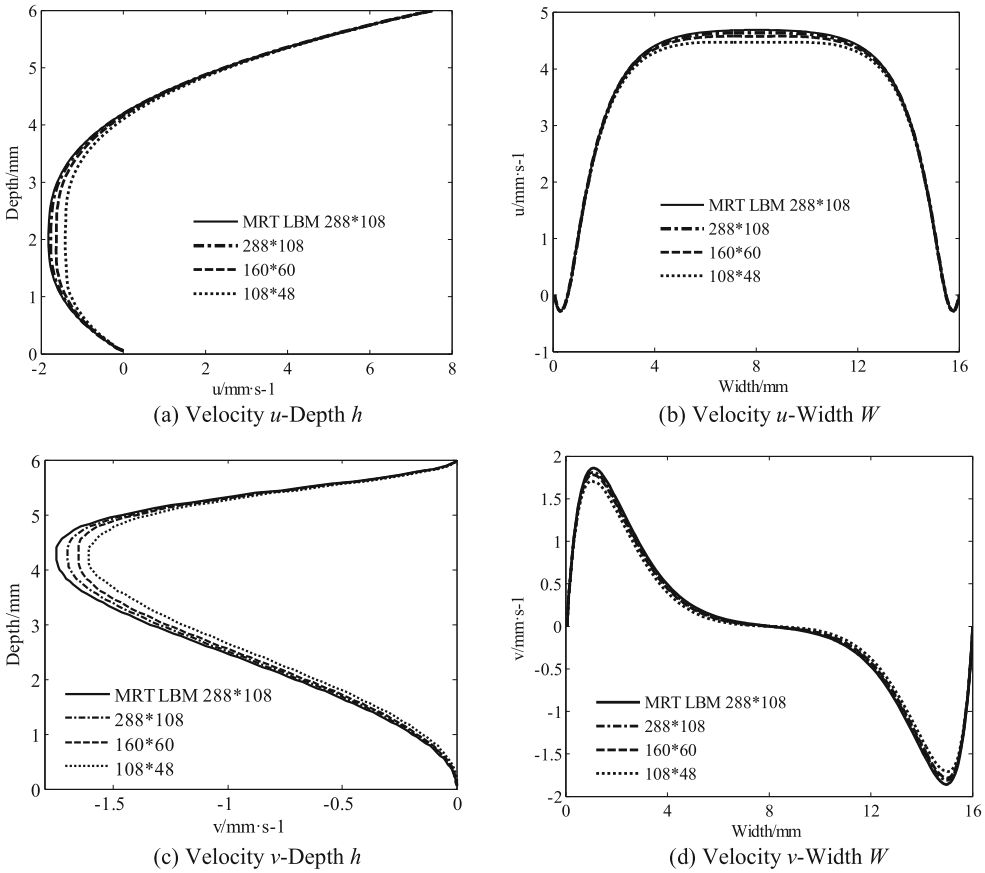

(a) Velocity u-Depth h

(b) Velocity u-Width W

(c) Velocity v-Depth h

(d) Velocity v-Width W

in Fig. 7. The lattice number of MRT-LBM is 288 × 108, and the lattice numbers of modified method are 288 × 108, 160 × 60, and 108 × 48, respectively.

Figure 7a, b shows the relationships between the velocity u with the screw depth and the screw width, respectively. In Fig. 7a, the lines correspond to the case where the screw width is 8 mm, and in Fig. 7b, the lines correspond to the screw depth of 5.4 mm. Figure 7c, d shows the relationships between the velocity v with the screw depth and the screw width, respectively. In Fig. 7c, the lines correspond to the case where the screw width is 14.4 mm, and in Fig. 7b, the lines correspond to the screw depth of 3 mm.

Conclusion

We proposed a modified lattice Boltzmann method for Herschel-Bulkley fluids, which could improve the stability of the simulation. Then, tested the method via Poiseuille flow. The calculation of the relative errors showed that with the increasing of the lattice number, the errors could be reduced to 0.1 %. Also the solutions of the shear-thinning fluids and the shear-thickening fluids presented the same trends. Furthermore, the region of the low-shear rate had no effect on the relative error. But the relative error was affected by the power law index greatly. Finally, we applied the method into the simulation of the cement paste flow in 3D printing extruder. Comparing the solution of the method with that of MRT-LBM, it could get a consistent result.

Acknowledgments This work was supported by the National Natural Science Foundation of China (grant no. 51635003) and China Torch Program Industrialization Guide Project (grant no. 2014GH040527).

References

Alexandrou AN, McGilvreay TM, Burgos G (2001) Steady Herschel–Bulkley fluid flow in three-dimensional expansions. J Non-Newton Fluid 100:77–96

Ansumali S, Karlin IV (2002a) Entropy function approach to the lattice Boltzmann method. J Stat Phys 107(1–2):291–308

Ansumali S, Karlin IV (2002b) Single relaxation time model for entropic lattice Boltzmann methods. Phys Rev E 65:056312

Ashorynejad HR, Mohamad AA, Sheikholeslami M (2013) Magnetic field effects on natural convection flow of a nanofluid in a horizontal cylindrical annulus using Lattice Boltzmann method. Int J Therm Sci 64:240–250

Boyd J, Buick JM, Green S (2007) Analysis of the Casson and Carreau-Yasuda non-Newtonian blood models in steady and oscillatory flows using the lattice Boltzmann method. Phys Fluids 19:093103

Boyd J, Buick J, Green S (2006) A second-order accurate lattice Boltzmann non-Newtonian flow model. J Phys A-Math Theor 39:14241

Buick JM, Cosgrove JA (2006) Numerical simulation of the flow field in the mixing section of a screw extruder by the lattice Boltzmann model. Chem Eng Sci 61:3323–3326

Buick JM (2009) Lattice Boltzmann simulation of power-law fluid flow in the mixing section of a single-screw extruder. Chem Eng Sci 64:52–58

Cesaretti G, Dini E, Kestelier XD, Colla V (2014) Building components for an outpost on the lunar soil by means of a novel 3D printing technology. Acta Astronaut 93:430–450

Chai Z, Shi B, Guo Z, Rong F (2011) Multiple-relaxation-time lattice Boltzmann model for generalized Newtonian fluid flows. J Non-Newton Fluid 166:332–342

Conrad D, Schneider A, Böhle M (2014) A viscosity adaption method for Lattice Boltzmann simulations. J Comput Phys 276:681–690

Cruz DOA, Pinho FT (2012) Analysis of isothermal flow of a Phan-Thien-Tanner fluid in a simplified model of a single-screw extruder. J Non-Newton Fluid 167:95–105

D'Humières D (2002) Multiple-relaxation-time lattice Boltzmann models in three dimensions. Philos T R Soc A 360:437–451

Gabbanelli S, Drazer G, Koplik J (2005) Lattice Boltzmann method for non-Newtonian (power-law) fluids. Phys Rev E 72:046312

Guo Z, Zhao TS, Shi Y (2005) A lattice Boltzmann algorithm for electro-osmotic flows in microfluidic devices. J Chem Phys 122:144907

Kefayati GHR (2014a) FDLBM simulation of magnetic field effect on natural convection of non-Newtonian power-law fluids in a linearly heated cavity. Powder Technol 256:87–99

Kefayati GHR (2014b) FDLBM simulation of magnetic field effect on non-Newtonian blood flow in a cavity driven by the motion of two facing lids. Powder Technol 253:325–337

Kim SJ, Kwon TH (1995) A numerical and experimental study of three-dimensional transport in the channel of an extruder for polymeric materials. Powder Technol 85:227–239

Malaspinas O, Courbebaisse G, Deville M (2007) Simulation of generalized Newtonian fluids with the lattice Boltzmann method. Int J Mod Phys C 18:1939–1949

Mitsoulis E (2007) Flows of viscoplastic materials: models and computations. Rheol Rev 2007:135–178

Mohamad AA (2011) Lattice Boltzmann method: fundamentals and engineering applications with computer codes. Springer Science & Business Media,

Papanastasiou TC, Boudouvis AG (1997) Flows of viscoplastic materials: models and computations. Comput Struct 64:677–694

Pegna J (1997) Exploratory investigation of solid freeform construction. Automat Constr 5:427–437

Pontrelli G, Ubertini S, Succi S (2009) The unstructured lattice Boltzmann method for non-Newtonian flows. J Stat Mech-Theory E 2009:P06005

Sastrohartono T, Jaluria Y, Esseghir M, Sernas V (1995) Development of numerical simulation methods and analysis of extrusion processes of particle-filled plastic materials subject to slip at the wall. Int J Heat Mass Tran 38:1957–1973

Seta T, Takahashi R (2002) Numerical stability analysis of FDLBM. J Stat Phys 107:557–572

Sheikholeslami M, Gorji-Bandpy M, Ganji DD (2014) Lattice Boltzmann method for MHD natural convection heat transfer using nanofluid. Powder Technol 254:82–93

Shen C, Tian DB, Xie C, Fan J (2003) Examination of the LBM in simulation of microchannel flow in transitional regime. 1st International Conference on Microchannels and Minichannels. American Society of Mechanical Engineers 405–410

Spasov M, Rempfer D, Mokhasi P (2009) Simulation of a turbulent channel flow with an entropic lattice Boltzmann method. Int J Numer Meth Fl 60:1241–1258

Wang CH, Ho JR (2008) Lattice Boltzmann modeling of Bingham plastics. Physica A 387:4740–4748

Wang W, Liu Z, Jin Y, Cheng Y (2011) LBM simulation of droplet formation in micro-channels. Chem Eng J 173:828–836

Yuan Y, Rahman S (2016) Extended application of lattice Boltzmann method to rarefied gas flow in micro-channels. Physica A 463:25–36

Zhen-Hua B-CS, Lin Z (2006) Simulating high Reynolds number flow in two-dimensional lid-driven cavity by multi-relaxation-time lattice Boltzmann method. Chin Phys 15:1855

Zhang J, Johnson PC, Popel AS (2008) Red blood cell aggregation and dissociation in shear flows simulated by lattice Boltzmann method. J Biomech 41:47–55

Zocca A, Colombo P, Gomes CM, Günster J (2015) Additive manufacturing of ceramics: issues, potentialities, and opportunities. J Am Ceram Soc 98:1983–2001